Microstructure of erbium-implanted Si

D. J. Eaglesham, J. Michel, E. A. Fitzgerald, D. C. Jacobson, J. M. Poate,
J. L. Benton, A. Polman, Y.-H. Xie, and L. C. Kimerling
AT&T Bell Laboratories, 600 Mountain Avenue, Murray Hill, New Jersey 07974

(Received 28 November 1990; accepted for publication 22 March 1991)

A study is presented of the relation between microstructure and 1.54 μm photoluminescence (PL) in high-energy ion-implantated Er in Si as a function of implant dose, energy, and temperature and subsequent anneal. Transmission electron microscopy (TEM) of material implanted at 500 keV and >100 °C and annealed at 900 °C to activate the Er PL suggests the solubility of Er in Si to be $\approx 1.3 \pm 0.4 \times 10^{18}$ cm^{-3} at 900 °C. Precipitates take the form of platelets (probably $ErSi_2$) $\approx$100–300 Å in diameter and $\approx$10 Å thick. The 1.54 μm PL saturates at $\approx 5 \times 10^{17}$ cm^{-3}, before the apparent solubility limit. Layers in which the Si is fully amorphized and subsequently regrown by solid phase epitaxy during an anneal show increased Er incorporation in the crystalline Si but segregation at the amorphous-crystalline interface. In buried amorphous layers regrown from top and bottom, segregation leads to a line of high Er concentration near the center of the layer: Regrowth from a single interface leads to a segregation pileup of Er at the interface until the precipitation threshhold is reached.

The attainment of efficient light emission from Si for optoelectronic integration is one of the holy grails of Si technology.[1] Recently Er in Si has begun to attract considerable interest for its potential to give high-efficiency sharp luminescence at 1.54 μm under optical pumping [e.g., see Refs. 2–7]. We have now demonstrated that high-energy implantation of Er ions leads to efficient photoluminescence (PL) and electroluminescence (EL) at low temperatures,[8] with sharp PL even at room temperature.[9] In order to optimize the optoelectronic properties of this system it is essential to understand the behavior of the microstructure under various implant and annealing conditions. In this letter we present the first data on the solubility, segregation and precipitation behavior of Er-implanted Si over most of the range of interest.

Implants of Er^+ into Si(100) wafers were carried out at temperatures ranging from room temperature to 300 °C for ion energies of 0.5–5.0 MeV. A variety of anneals were carried out, although for most of this study we have concentrated on the region near 900 °C which tends to maximize the PL.[3,9] Although the presence of O in Czochralski (CZ) Si has been reported to enhance the luminescence response,[7] implants were carried out into both CZ and float-zone (FZ) Si in order to establish whether O affects the precipitation kinetics. The microstructure of both as-implanted and annealed material was studied using transmission electron microscopy (TEM) and Rutherford backscattering spectrometry and channeling (RBS) in order to establish the "equilibrium" phase behavior and the role of implantation damage.

Erbium incorporation in Si is limited by precipitation. Figure 1 shows 1.2×10^{14} cm^{-2} 500 keV Er in CZ Si(100) (implanted at 130 °C so that the implant dose lies below the threshhold for amorphization) following a 900 °C anneal. The features seen in this (400) weak-beam image near the end-of-range of the Er ions show contrast similar to dislocation loops but are visible in all reflections, and appear dark in bright field images away from strongly diffracting orientations. The strong strain contrast observed within the loops implies that they are not dislocation loops or regions of faulted or twinned Si. Tilting experiments show that these "loops" lie on [111] planes. These defects clearly differ from the usual ion-implantation damage in Si, which can include dislocation loops, stacking fault loops, and [311] defects in high O concentrations. The absence of a $g \cdot b = 0$ criterion, the absorption contrast at weakly diffracting orientations and the strong inside-outside contrast at $\pm g$ are all consistent with these defects being Er-rich precipitates, the most likely phase from the Er-Si phase diagram[10] being $ErSi_2$ (or $ErSi_{2-x}$, sometimes designated Er_3Si_5).[11] These precipitates clearly adopt a platelet morphology on [111] with lateral dimensions of $\approx$100–300 Å and a thickness normal to the plane below the ($\approx$30 Å) resolution of weak-beam images at large deviation parameters (not shown). Figure 2 shows a high-resolution image along [110] in which one of these platelets can be seen

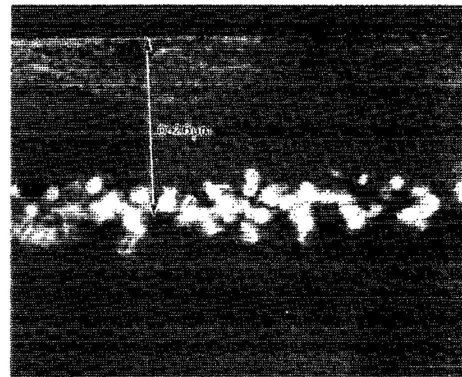

FIG. 1. Precipitation in Er-implanted Si. TEM image [(400) weak-beam at small deviation] of cross section of sample implanted to a peak concentration of 6.6×10^{18} cm^{-3} and annealed at 900 °C for 30 min. The small loop-like features lie around the peak in the Er concentration, are visible in all reflections, and show absorption contrast away from strong diffracting conditions.

 © 1991 American Institute of Physics

Downloaded 15 Sep 2003 to 131.215.237.132. Redistribution subject to AIP license or copyright, see http://ojps.aip.org/aplo/aplcr.jsp

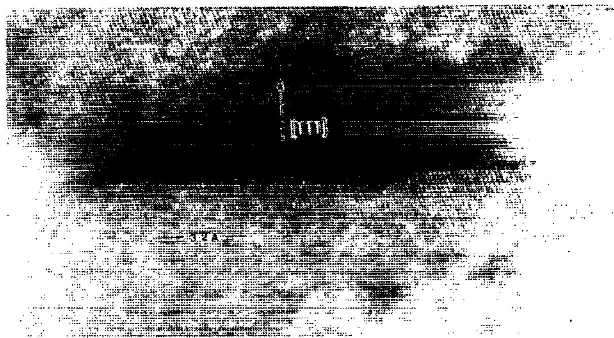

FIG. 2. Precipitate seen edge-on: High-resolution image along ⟨011⟩ showing the platelet morphology. The defect is >400 Å in diameter and has an apparent width of 3 Si [111] planes (9.4 Å). The structure within this region differs from that outside for all defoci, and is always darker in thick regions. The platelet appears to involve an inclusion of several planes of a structure other than Si.

edge-on. As expected from diffraction contrast, the defect has no well-defined fault vector in the Si matrix, and there appear to be several planes which adopt a structure different from the Si matrix. Since the precipitates are only a few atomic planes thick the precipitating phase is not structurally well defined. We conclude that, at high concentrations, Er precipitates in the form of platelets a few atoms thick which lie on the Si [111] and probably resemble $ErSi_2$ in structure.

The solubility of Er in Si is clearly important in understanding the luminescence properties of this system. Figure 3 shows the microstructure of Si implanted with 500 keV Er^+ to doses of 1.7, 2.9, 5.8, 8.7, and 11.6 $\times 10^{13}$ cm^{-2} at 130 °C and annealed to 900 °C for 30 min. RBS measurements of the range (1840 Å) and straggle (520 Å) of 500 keV Er at much higher doses show that these correspond to concentrations of 1.0, 1.65, 3.3, 4.9, and 6.6

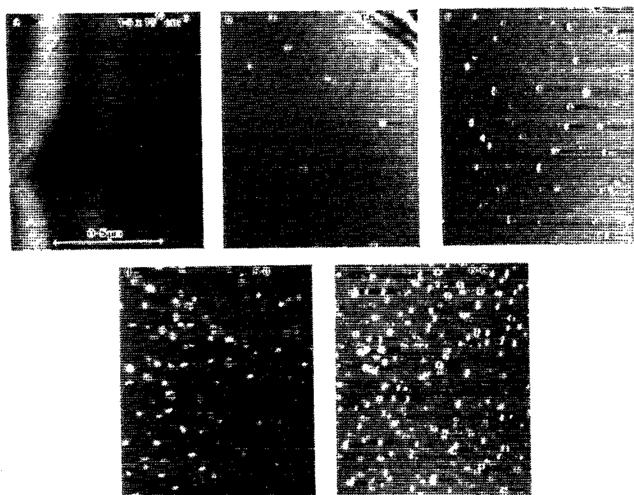

FIG. 3. Precipitate density at different doses. 500 keV Er^+ implants to concentrations (at the peak of the implanted distribution) of 1.0, 1.65, 3.3, 4.9, and 6.6×10^{18} cm^{-3}, following a 30 min anneal at 900 °C. Plan-view TEM [weak-beam images in a (220) reflection]: The steep increase in density above 1.0×10^{18} cm^{-3} implies that this is near the solubility limit.

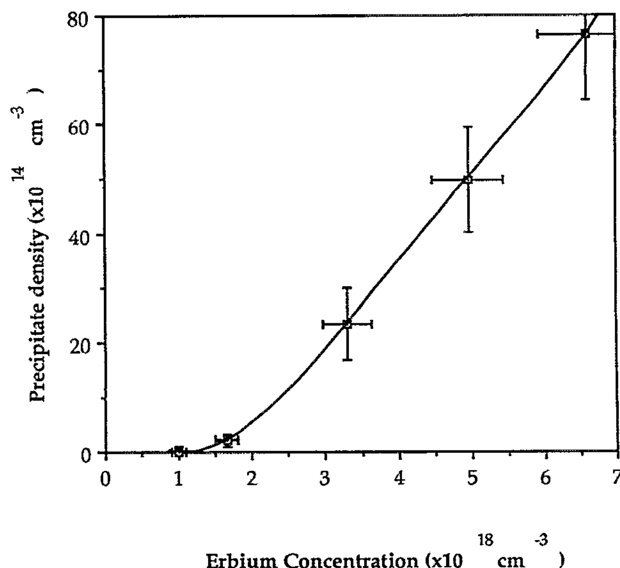

FIG. 4. Precipitate density from Fig. 3 as a function of peak concentration: The solubility suggested by extrapolation is $1.3\pm 0.4\times 10^{18}$ cm^{-3}.

$\times 10^{18}$ cm^{-3} at the peak of the Er implant. These plan-view TEM images [(220) weak-beam] clearly show a rapid increase in the precipitate density beyond 1.0×10^{18} cm^{-3}, as is shown graphically in Fig. 4, where extrapolation assuming either a linear or quadratic concentration dependence gives an intercept of either 1.5×10^{18} or 1.1×10^{18} cm^{-3}. Annealing for longer times does not significantly affect the microstructure observed in dark-field TEM (although the precipitates may increase in thickness). Equating this threshhold for precipitation with an equilibrium bulk solubility limit is complicated, since the as-implanted concentration distribution of Er is rather narrow, so that in these plan-view images the apparent precipitate density is an average through a layer of varying Er concentration. In addition, some redistribution of the Er profile may occur during the 900 °C anneal. We do in fact observe a small dependence of the value of this threshhold on the implant energy (implying that the onset of precipitation may depend on the width of the initial Er distribution). However, for practical purposes the threshhold for precipitation may be a more useful number than the bulk equilibrium solubility. Similar experiments in FZ Si implanted at room temperature show an onset of precipitation near the same concentration and identical contrast at precipitates.

Comparison with PL measurements (reported in greater detail elsewhere[9]) shows two very surprising features. First, the PL, after a linear increase at low concentrations, shows an initial saturation at concentrations $\approx 5\times 10^{17}$ cm^{-3}, well below the solubility limit. This seems to imply that higher concentrations lead to different point defects which are less efficient in emission (possibly as the Er concentration exceeds the oxygen). Second, at the onset of precipitation we see an apparent further two-fold *increase* in the PL between 2 and 4×10^{18} cm^{-3}, followed by a decrease to approximately the 5×10^{17} cm^{-3} level at 7×10^{18} cm^{-3}. Either the precipitates are emitting

Downloaded 15 Sep 2003 to 131.215.237.132. Redistribution subject to AIP license or copyright, see http://ojps.aip.org/aplo/aplcr.jsp

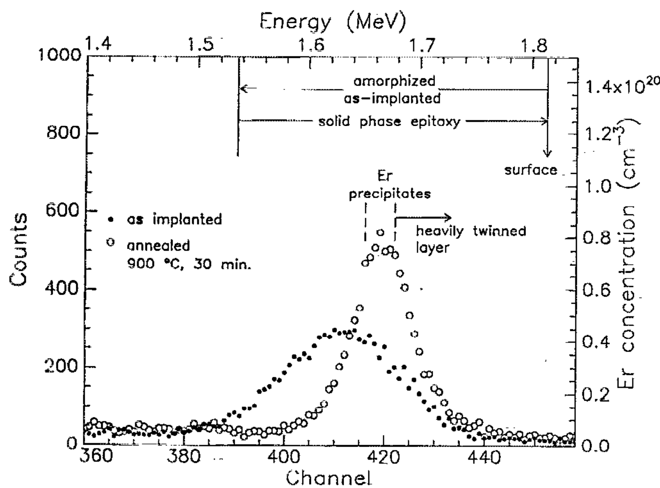

FIG. 5. Er segregation in Si at a dose where the implant fully amorphized the Si to the end of range. RBS spectrum as-implanted, and following SPE at 900 °C showing Er segregation at the amorphous-crystalline interface to form a line of high concentration. Beyond this line of high concentration, further SPE has led to highly defective Si with a χ_{min} of $>70\%$. Comparison with TEM shows that SPE occurs with low defect levels up to the threshhold for precipitation, and subsequent SPE is heavily twinned.

light at 1.54 μm, or they alter the background defect population so as to enhance the efficiency of dissolved Er. The absence of a strong PL signal from FZ Si containing precipitates (where Er in solution does not show PL) suggests that the latter is the more plausible explanation.

While it should be noted that in many of the published studies of Er-implanted Si amorphizing and nonamorphizing implant doses have not been clearly distinguished, the implants used above to study the incorporation of Er are all carried out at elevated temperature (130 °C), and lie below the threshhold for amorphization at this temperature. However, we have also studied the incorporation of Er under amorphizing (high dose) Er implants at room temperature and MeV energies for two limiting cases. When the dose is high enough to amorphize to the surface, annealing leads to solid phase epitaxy (SPE) from the end-of-range. RBS (Fig. 5) shows that the Er appears to segregate to form a peak. The tail in the spectra is an artifact of the RBS technique and would correspond to an Er concentration of 3×10^{18} cm^{-3}; this sets an upper limit on the Er incorporation in the crystal. In TEM, we observe defect-free regions extending from the end of range (the as-implanted amorphous-crystal interface) to the approximate position of the Er peak seen in RBS; at this depth a line of precipitates is observed, and all subsequent growth is heavily defective, with stacking faults and twins extending to the surface. These results show a strong tendency of the Er to segregate during SPE, in spite of the low diffusion length we observe for Er diffusion even in amorphous Si at these temperatures. Similar observations of Sb segregation during SPE[12] have been linked to an "interfacial segregation" effect.[13] Segregation during SPE would offer a simple explanation of the migration of Er to the surface observed in some previous studies[14] (see also Ref. 6). At slightly lower implant doses the Si is not fully amorphized to the surface, and SPE during annealing takes place from both top and bottom of the amorphous layer. In these samples RBS shows a single sharp spike in the Er distribution, while TEM shows a low density of "hairpin" dislocations extending from top and bottom, to a single line of high Er content (not in the form of the usual precipitates).

In conclusion, we have studied the incorporation of Er into Si by ion implantation. The threshhold for precipitation is $\approx 1.3\pm0.4\times10^{18}$ cm^{-3} at 900 °C in both CZ and FZ Si, and precipitation takes the form of thin platelets $\approx$300 Å in diameter and $\approx$10 Å thick; these platelets are probably similar to $ErSi_2$ in structure. In CZ Si the PL saturates before the onset of precipitation, indicating a change in character of the Er point defects with increasing concentration. The onset of precipitation enhances the observed PL yield, but since precipitates in FZ Si do not luminesce, this is probably linked to enhanced emission from Er in solution. Amorphization during the implant leads to Er segregation during SPE in the subsequent anneal: For high Er concentrations the segregating Er can precipitate, leading to highly defective Si.

[1] See e. g., A. Tennyson, *The Holy Grail and Other Poems* (R. R. Clarke, London, 1869).
[2] H. Ennen, J. Schneider, G. Pomrenke, and A. Axman, Appl. Phys. Lett. **43**, 943 (1983).
[3] H. Ennen, G. Pomrenke, A. Axman, K. Eisele, W. Haydl, and J. Schneider, Appl. Phys. Lett. **46**, 381 (1985).
[4] P. B. Klein and G. S. Pomrenke, Electron. Lett. **24**, 1502 (1988).
[5] Y. S. Tsang, K. C. Heasman, W. P. Gillin, and B.J. Sealy, Appl. Phys. Lett. **55**, 432 (1989).
[6] Y. S. Tsang and B. J. Sealy, J. Appl. Phys. **68**, 2530 (1990).
[7] P. N. Fannevec, H. L'Haridon, D. Moutonnet, M. Salvi, and M. Gauneal, Jpn. J. Appl. Phys. **29**, L524 (1990).
[8] Y.-H. Xie, J. L. Benton, D. C. Jacobson, R. F. Ferrante, D. J. Eaglesham, E. A. Fitzgerald, J. Michel, J. M. Poate, and L. C. Kimerling (unpublished).
[9] J. Michel, J. L. Benton, R. F. Ferrante, D. C. Jacobson, D. J. Eaglesham, E. A. Fitzgerald, Y.-H. Xie, J. M. Poate, and L. C. Kimerling (unpublished).
[10] W. G. Moffat, ed., *Handbook of Binary Alloy Phase Diagrams*, (Business Growth Services, General Electric Co., Schenectady, NY, 1976).
[11] A. Jandelli, A. Palenzona, and G. L. Olcese, J. Less Common Metals **64**, 213 (1979).
[12] J. S. Williams, in *Surface Modification and Alloying by Laser, Ion, and Electron Beams*, NATO Conf. Ser. IV, Mat. Sci. edited by J. M. Poate, G. Foti, and D. C. Jacobson (Plenum, New York, 1983), Vol. 8, p. 133.
[13] W. Slijkerman, private communication; Ph.D thesis, FOM Institute, Amsterdam, Netherlands.
[14] Y. S. Tang Z. Jinping K. C. Heasman, and B. J. Sealy, Solid State Commun. **72**, 991 (1989).

Downloaded 15 Sep 2003 to 131.215.237.132. Redistribution subject to AIP license or copyright, see http://ojps.aip.org/aplo/aplcr.jsp